Reply to Anonymous Referee #2

This manuscript investigates the impacts of anthropogenic aerosols on a winter snowfall event over the Guanzhong Basin using WRF-Chem, with a focus on disentangling aerosol–radiation interactions (ARIs) and aerosol–cloud interactions (ACIs). The topic is scientifically important, especially given the large uncertainties in aerosol–precipitation interactions under polluted conditions. The study is generally well structured, and the model reasonably reproduces observed pollutants and precipitation. The attempt to separate ARI and ACI contributions and the identification of contrasting responses between GZB and surrounding regions are valuable. However, the manuscript still has several critical issues in physical interpretation, experimental design, and result robustness, which need to be addressed before publication.

1 Comment: Wet scavenging refers to the effect of precipitation on aerosols, rather than the influence of aerosols on precipitation. In addition, the phrase "decreased solar radiation" is not appropriate to describe the impact of aerosols on precipitation.

Response: We have removed "wet scavenging" from the sentence and have revised "decreased solar radiation" to a more accurate description in lines 42-44 as follows,

"*Past studies have proposed many mechanisms about aerosol effects on precipitation, such as the positive precipitation-aerosol relationships attributed to invigoration effect (e.g., Khain et al., 2005; Pinsky et al., 2013; Rosenfeld et al., 2008), the negative aerosol effect on precipitation due to cloud water competition (e.g., Albrecht, 1989; Rosenfeld, 1999), and ARIs that reduce solar radiation down to the surface and modify atmospheric temperature profiles (e.g., Ackerman et al., 2000; Koren et al., 2004).*"

2 Comment: As shown in Figure 3, compared with the simulation results of $PM_{2.5}$, O_3, and NO_2, the simulation errors of SO_2 are relatively larger. The authors should provide a clear explanation for these discrepancies.

Response: We have added a concise explanation specifically for SO_2 in lines 198-205 of the revised manuscript as follows,

"*However, the model does not show good performance in simulating the SO_2 temporal variation, with an IOA of 0.25. The larger discrepancy for SO_2 mainly results from the sensitivity of point-source SO_2 simulations to meteorological uncertainties. The transport and dispersion of SO_2 from point sources (i.e., power plants and industrial* *facilities) are highly sensitive to the accuracy of simulated wind fields (Hu et al., 2022). In the GZB, complex terrain and weak synoptic forcing further increase the uncertainty in meteorological simulations (Bei et al., 2017b). Additionally, parameterizations of SO_2 oxidation, including aqueous-phase and heterogeneous pathways, under the persistent high-RH conditions during this snowfall event also introduces further uncertainties (Travis et al., 2025).*"

Bei, N., Zhao, L., Xiao, B., Meng, N., and Feng, T.: Impacts of local circulations on the wintertime air pollution in the Guanzhong Basin, China, Sci. Total Environ., 592, 373–390, https://doi.org/10.1016/j.scitotenv.2017.02.151, 2017b.

Hu, Y., Zang, Z., Chen, D., Ma, X., Liang, Y., You, W., Pan, X., Wang, L., Wang, D., and Zhang, Z.: Optimization and evaluation of SO2 emissions based on WRF-Chem and 3DVAR data assimilation, Remote Sens., 14, 220, https://doi.org/10.3390/rs14010220, 2022.

Travis, K. R., Nault, B. A., Crawford, J. H., Kim, H., Chen, Q., Zheng, Y., Liu, T., Jimenez, J. L., Campuzano-Jost, P., Wennberg, P. O., Crounse, J. D., and Huey, L. G.: Year-round analysis of multiphase sulfate production in aerosol particles in East Asia, ACS ES&T Air, 2, 1758–1769, https://doi.org/10.1021/acsestair.5c00136, 2025.

3 Comment: The boundary between the Guanzhong Basin (GZB) and its surrounding areas (GZBs) should be added in all figures to improve readability. Furthermore, the comparison of accumulated precipitation results should be separated between GZB and GZBs to ensure that no systematic differences are overlooked.

Response: We have modified Figures 1, 2, 5, and 14 as suggested. We have also modified Figures 4 and 5 to increase the rain rate comparison over GZB and GZBs. We have added discussions in Lines 211-216 as follows,

"*Figure 4 provides the temporal variation of precipitation rates averaged at meteorological sites in GZB+GZBs from 26 to 28 January. The model generally reproduces the temporal evolution of the observed hourly precipitation, with NMBs of -3.3%, -7.4%, and -1.3% and IOAs of 0.85, 0.75, and 0.78 over GZB+GZBs, GZB, and GZBs, respectively. The observed five rainrate peaks are successfully reproduced in all regions, but the underestimation of the first and fifth rainrate peak is considerable in GZB+GZBs. Compared with GZB, the model exhibits better overall performance in GZBs, while a larger underestimation is found over GZB during periods of intense precipitation. These underestimations are likely related to the model's sensitivity to* *initial conditions and its performance during the spin up and decay stages of the event, respectively, especially given that the precipitation occurs on the periphery of the cold front where large scale forcing is weak (Liu et al., 2018; Lin et al., 2023). Additionally, the model also produces higher light precipitation during 27-28 January compared to the observations. As shown by Liu et al. (2024), the lack of a shallow convection scheme at gray zone resolutions (i.e., 6 km) allows excessive low level moisture to accumulate and prematurely convert to light precipitation under stratiform conditions. These localized discrepancies do not compromise the model's overall performance. The pattern comparison of the 3-day accumulative precipitation over the GZB and GZBs is shown in Figure 5. The model generally replicates the precipitation distribution compared to the observations (Figure 5a). For all stations in GZB+GZBs, the simulated accumulated precipitation agrees reasonably well with observations, with an NMB of -3.7% and an IOA of 0.85 (Figure 5b). When evaluated separately, the model yields NMBs of -10.2% and -1.3% over GZB and GZBs, respectively, indicating that the underestimation is mainly concentrated within the basin region. Nevertheless, the relatively high IOAs of 0.89 and 0.85 over GZB and GZBs suggest that the model adequately captures the spatial variability of precipitation in both regions.*"

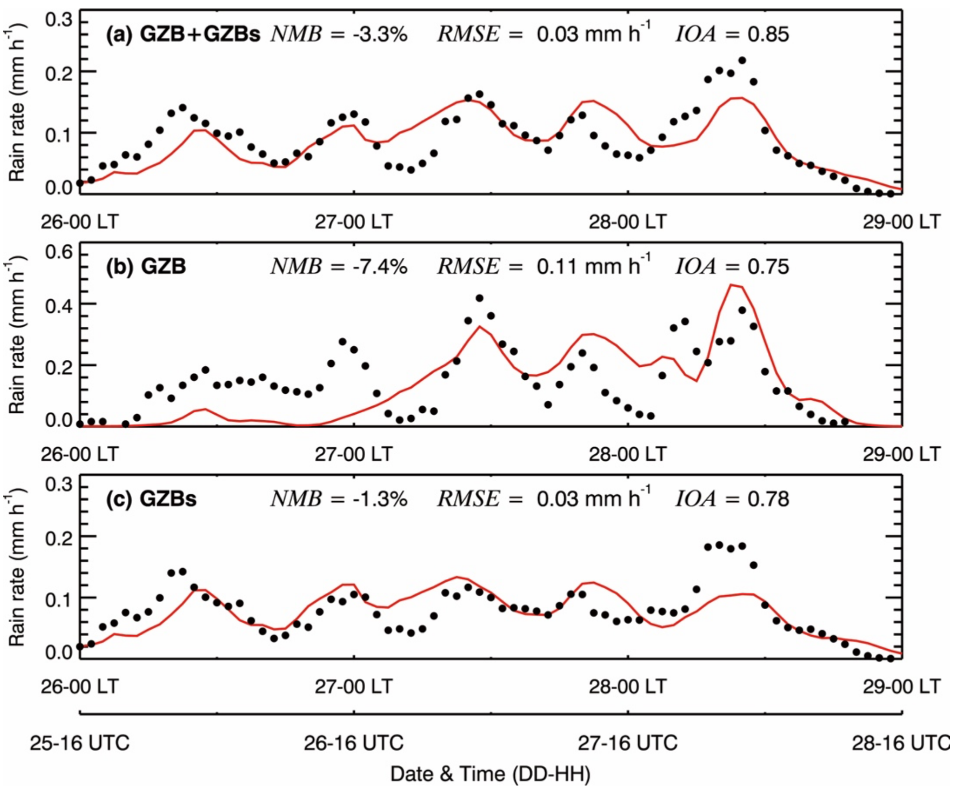

Figure 4: Comparison of observed (black dots) and simulated (solid red lines) diurnal profile of hourly rain rate averaged at monitoring sites in (a) GZB+GZBs, (b) GZB, and (c) GZBs from 26 to 28 January 2022.

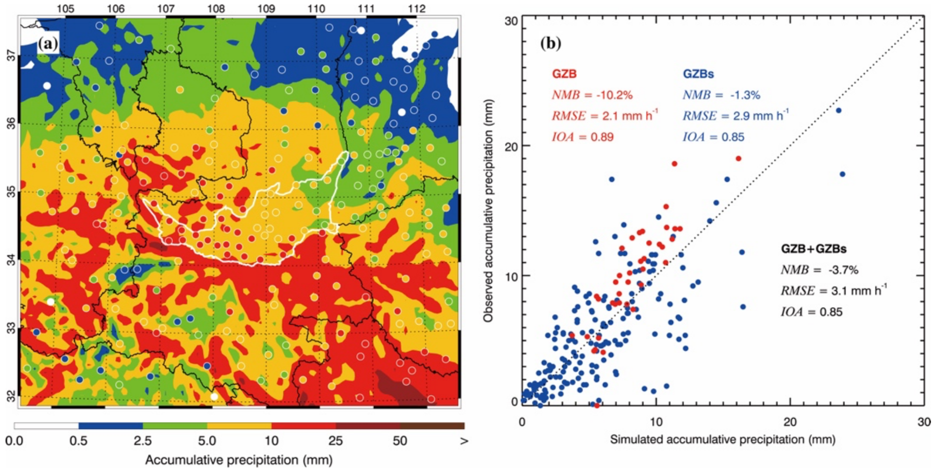

Figure 5: (a) Pattern comparisons of simulated (color counters) vs. observed (colored dots) accumulative precipitation, and (b) scatter plot of simulated and observed accumulative precipitation in GZB, GZBs, and GZB+GZBs from 26 to 28 January 2022. The white contour outlines the GZB, and the area outside of GZB in (a) is referred to as GZBs.

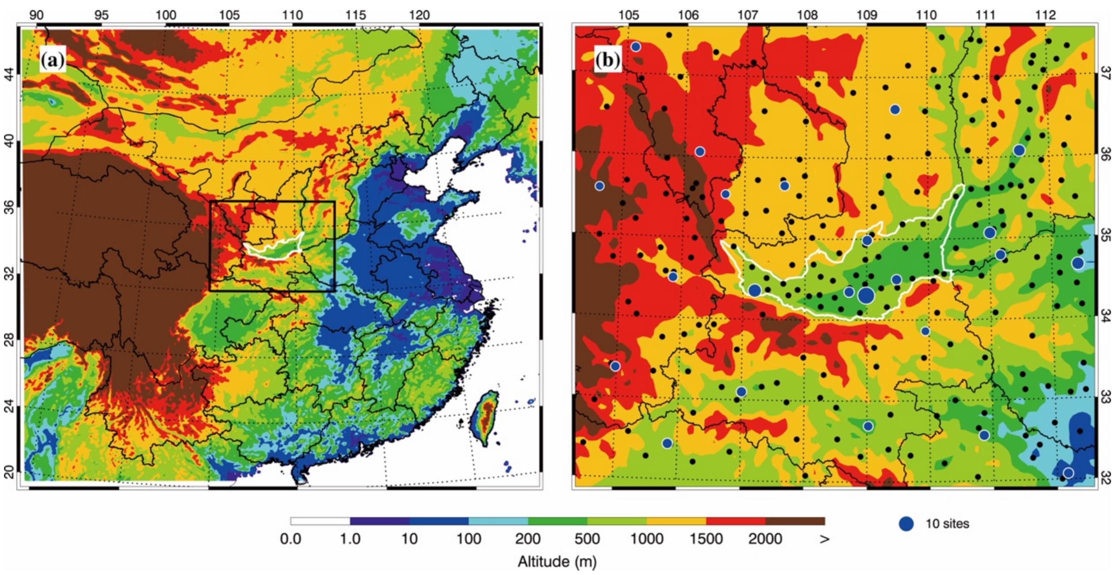

Figure 1: (a) WRF-Chem simulation domain with topography and (b) Guanzhong basin (GZB) and its surrounding areas (GZBs). In (b), the black dots denote the meteorological sites with rain gauge and the blue dots denote centers of cities with air pollutants observations and the size of blue circles denotes the number of ambient monitoring sites of cities. The white contour outlines the GZB and the area outside of GZB in (b) is referred to as GZBs.

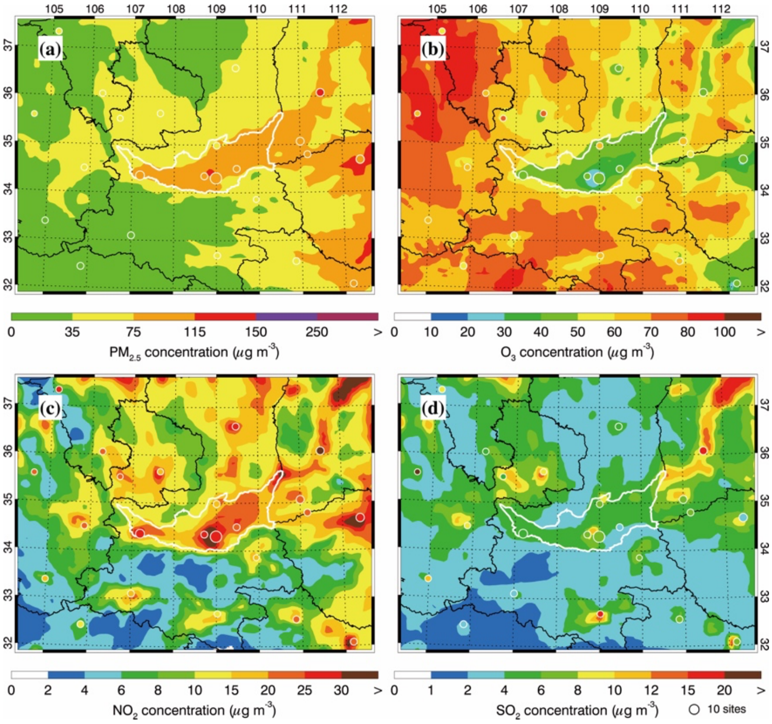

Figure 2: Pattern comparisons of simulated (color counters) vs. observed (colored dots) average near-surface mass concentrations of (a) $PM_{2.5}$, (b) O_3, (c) NO_2 and (d) SO_2 from 26 to 28 January 2022. The white contour outlines the GZB and the area outside of GZB in panels is referred to as GZBs.

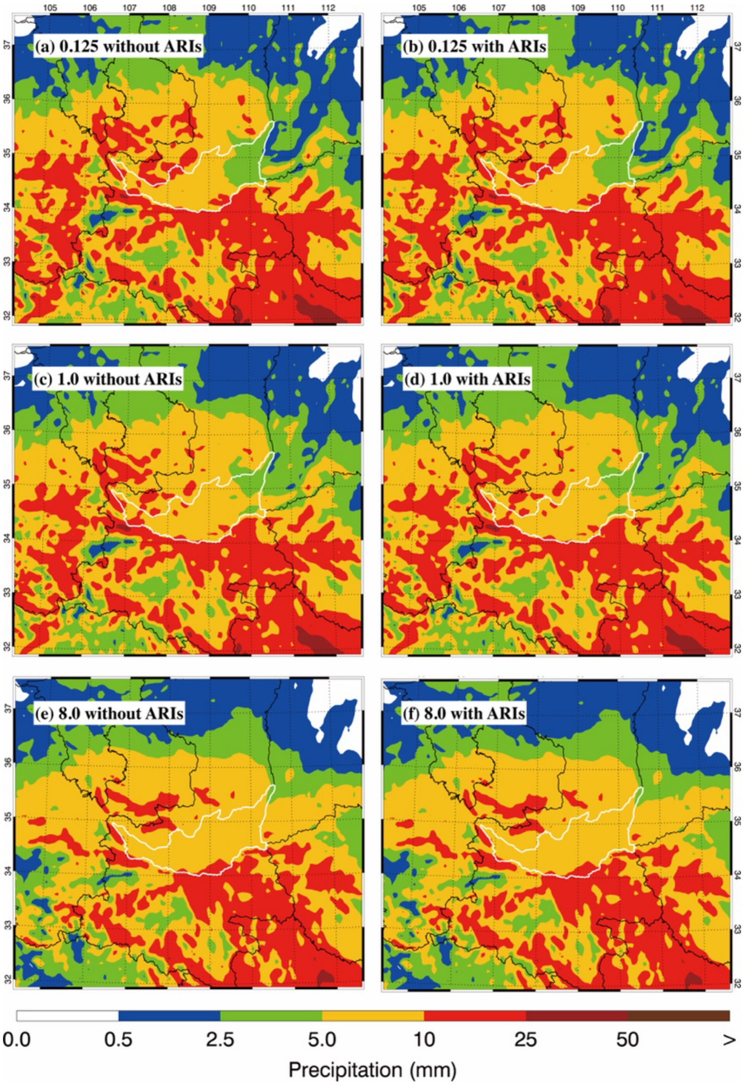

Figure 14: Distribution of accumulative precipitation from 26 to 28 January 2022 for various scale factor of anthropogenic emissions when ARIs are (a), (c), and (e) excluded and (b), (d), and (f) included. The white contour outlines the GZB. The white contour outlines the GZB and the area outside of GZB in panels is referred to as GZBs.

4 Comment: The distinction between $PM_{2.5}$ (in Section 3.2) and near-surface $PM_{2.5}$ (in Section 3.3) is unclear. The authors should explicitly state how near-surface $PM_{2.5}$ concentrations are calculated from the model simulation results.

Response: We thank the reviewer for this comment. We apologize for the unclear terminology in the original manuscript. In both Sections 3.2 and 3.3, "[$PM_{2.5}$]" refers to the near-surface $PM_{2.5}$ concentration derived from the lowest model layer. To avoid confusion, we have clarified this definition where "[$PM_{2.5}$]" is first introduced in the manuscript (Line 166), which now reads:

"*Meanwhile, despite the occurrence of the snowfall event, the observed near-surface $PM_{2.5}$ concentrations ([$PM_{2.5}$]) are still high during the three days……*"

For consistency, "[$PM_{2.5}$]" is used throughout the remainder of the manuscript to represent near-surface $PM_{2.5}$ concentrations, and redundant repetitions of "near-surface" have been removed.

5 Comment: As shown in lines 190–193 and Figure 6, the statement "the single scattering albedo is about 0.88, indicating a strong absorbing atmosphere over GZB+GZBs" requires more careful validation: First, when comparing absorbing AOD with total AOD, the absorbing component contributes only about 10%, suggesting that non-absorbing aerosols may dominate. Second, as mentioned above, aerosols can decrease PBLH through ACIs, while absorbing aerosols can heat the near-surface atmosphere by absorbing solar radiation, potentially leading to an increase in PBLH. More detailed analysis should therefore be provided, including aerosol layer height, temperature profiles, and related diagnostics.

Response: We thank the reviewer for this careful and insightful comment.

For the aerosol absorption, we have revised the sentence in lines 247-249 to: "*The average AOD and AAOD at 550nm in GZB+GZBs are 0.58 and 0.071 in the CNTL case, respectively, and the single scattering albedo at 550nm is about 0.88, indicating a moderately absorbing component within an otherwise scattering-dominated aerosol population over GZB+GZBs.*"

Regarding the relationship between absorbing aerosols and PBL development, we have revised the manuscript and added the following discussion in lines 262-266 and lines 268-286 as follows,

"*Consistent with these studies, the ARI-induced temperature response in the present simulation is characterized by cooling below approximately 1.8 km and weak warming aloft (Figure 7a). The lower-atmospheric cooling is mainly caused by reduced surface solar radiation which decreases the surface sensible heat, whereas the elevated warming is associated with aerosol absorption. The resulting thermal contrast enhances lower-tropospheric stability and suppresses turbulent mixing. Consequently, the average PBLH over GZB+GZBs decreases from about 450 m to 300 m with the AESF increasing from 0.125 to 8.0 in the F_BASE, but the warming layer is generally above 1.8 km and can extend to 7~8 km with the AESF exceeding 0.5. It is worth noting that the vertical distribution of aerosol-induced heating does not necessarily coincide with the vertical distribution of absorbing aerosols. As discussed by Wu et al. (2025), radiative heating depends not only on aerosol loading but also on the vertical structure of radiative fluxes, aerosol optical properties, and air density, particularly as well as the decreased surface sensible heat. Therefore, the weak warming above approximately*

1.8 km shown in Figure 7a should be interpreted as the integrated response of aerosol–radiation interactions rather than a direct reflection of aerosol concentration at a given altitude."

6 Comment: Absorbing aerosols typically induce significant heating at the layer where they are present, leading to cooling of the atmosphere below, while exerting relatively minor influence above. However, as shown in Figure 7, no distinct warming layer is observed. In addition, although the positive and negative variations in temperature and water vapor content appear relatively consistent, the patterns of vertical velocity differ. For instance, in some regions both cooling and warming are evident, yet the corresponding vertical velocities remain positive. This discrepancy requires further clarification.

Response: We thank the reviewer for the careful examination of Figure 7. Regarding the indistinct warming layer and the apparent inconsistency between the temperature, water-vapor, and vertical-velocity responses, we have added discussions in lines 268-286 and lines 290-302 as follows,

"*It is worth noting that the vertical distribution of aerosol-induced heating does not necessarily coincide with the vertical distribution of absorbing aerosols. As discussed by Wu et al. (2025), radiative heating depends not only on aerosol loading but also on the vertical structure of radiative fluxes, aerosol optical properties, and air density, particularly as well as the decreased surface latent heat. Therefore, the weak warming above approximately 1.8 km shown in Figure 7a should be interpreted as the integrated response of aerosol–radiation interactions rather than a direct reflection of aerosol concentration at a given altitude. During the study period, the profile of vertical velocity shows occurrence of downdraft within the PBL and updraft above the PBL (Figure S3a). The cooling effect of ARIs within the near-surface atmosphere induces a downward motion and meanwhile an upward motion is generated above the PBL, which is resulted from the warming effect caused by absorbing aerosols and enhanced convergence by the ARI-induced downward motion (Figure 7b). The vertical velocity response shown in Figure 7b does not directly mirror the temperature anomalies at each height. Instead, it reflects a dynamical adjustment to the vertically contrasting radiative forcing. Aerosol scattering cools the lower atmosphere through surface dimming, while aerosol absorption produces weak warming above approximately 1.8 km. The resulting thermal contrast favors ascent above the PBL, while downward motion develops within the boundary layer due to the combined effects of enhanced* *lower-tropospheric stability and compensating subsidence associated with the ascent aloft. Consequently, ARIs strengthen downward motion in the lower atmosphere and upward motion aloft. These ARI-induced variations in divergence and water vapor flux are shown in Figure S5. ARIs induce divergence (positive values) below approximately 700 m and convergence (negative values) above this level, with the convergence strengthening as AESF increases. Correspondingly, negative water vapor flux anomalies occur within the divergent layer, indicating moisture export from the lower troposphere, while positive anomalies occur within the convergent layer aloft, indicating moisture accumulation. This circulation pattern contributes to the drying of the PBL. Therefore, the upward motion above the PBL is enhanced by ARIs and more warm and moist air in the lower layer is being transported upward. The ARI-enhanced downward motion within the near-surface atmosphere is subject to transporting more air in the upper layer downward, causing a dry and cold effect, as shown in Figure 7c.*"

7 Comment: The manuscript presents an interesting case study on aerosol impacts on snowfall using WRF-Chem, but the physical interpretation of aerosol–radiation interactions (ARIs) remains insufficiently supported. In particular, the study lacks a quantitative analysis of radiative heating rates or flux divergence, making it difficult to attribute the simulated temperature changes solely to ARIs rather than dynamical adjustments.

Response: We thank the reviewer for this important comment. We agree that Figure 7 does not isolate the instantaneous radiative heating rate or radiative flux divergence. Instead, the temperature differences shown in Figure 7a represent the total atmospheric response induced by ARIs. We have now clarified it in Lines 255-258 as follows:

"*Figure 7a shows the effect of ARIs on the temperature profile averaged in GZB+GZBs during the study period by differentiating the F_BASE and F_ARI0 under various aerosol conditions. It should be noted that the temperature anomalies shown in Figure 7a represent the total atmospheric response to ARIs, including both the direct aerosol radiative forcing and the subsequent dynamical adjustments, such as changes in vertical motion, heat transport, and boundary-layer mixing. ARIs decrease the air temperature of the low-level atmosphere, and the air temperature decrease is mainly concentrated below 1.8 km and becomes increasingly significant with decreasing height or increasing AESF (Figure 7a).*"

We have added a quantitative analysis of flux divergence and related discussions in lines 297-302 of the revised manuscript as follows, "*These ARI-induced variations in divergence and water vapor flux are shown in Figure S5. ARIs induce divergence (positive values) below approximately 700 m and convergence (negative values) above this level, with the convergence strengthening as AESF increases. Correspondingly, negative water vapor flux anomalies occur within the divergent layer, indicating moisture export from the lower troposphere, while positive anomalies occur within the convergent layer aloft, indicating moisture accumulation. This circulation pattern contributes to the drying of the PBL.*"

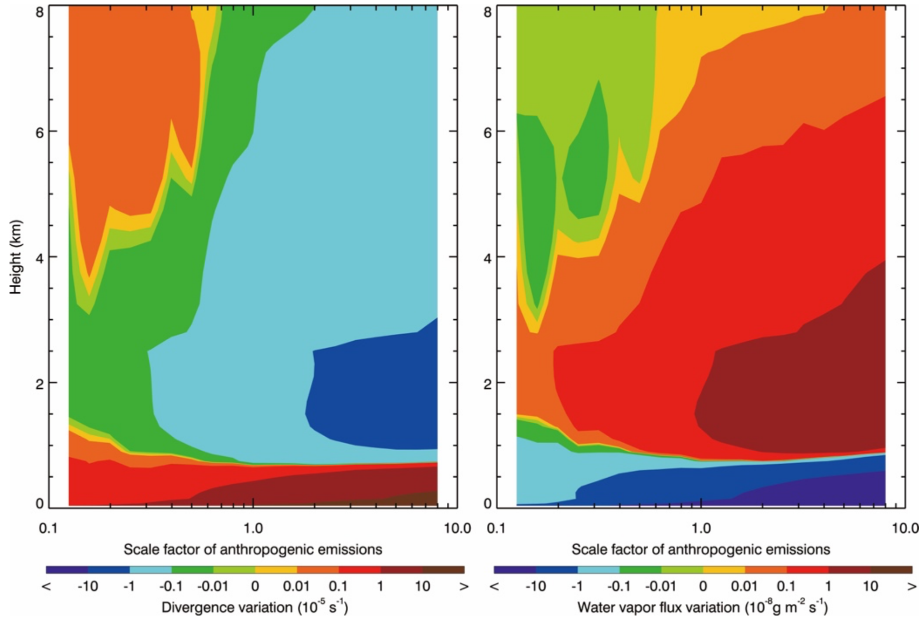

Figure S5: *Profile variation of horizontal (a) divergence and (b) water vapor flux averaged over GZB+GZBs from 26 to 28 January 2022 caused by ARIs, as a function of the scale factor of anthropogenic emissions. For the divergence variations, negative values indicate that ARIs enhance convergence, whereas positive values indicate enhanced divergence. For the water vapor flux variations, positive values indicate enhanced moisture inflow into the region, while negative values indicate enhanced moisture outflow from the study region.*

8 Comment: The separation of aerosol–radiation interactions (ARIs) and aerosol–cloud interactions (ACIs) using sensitivity experiments may introduce methodological uncertainties. Given the nonlinear coupling between radiation, thermodynamics, and microphysics, the simple differencing approach (F_BASE minus F_ARI0) may not fully isolate ARI effects. The authors should discuss the potential nonlinearity and associated uncertainties more explicitly.

Response: We have added discussions in lines 482-491 of the revised manuscript as "*The sensitivity experiment design used to separate ARIs and ACIs is subject to* *uncertainties arising from the nonlinear coupling between radiation, thermodynamics, and cloud microphysics. The differencing approach does not fully isolate pure ARIs but rather includes contributions from nonlinear interactions between ARIs and ACIs. While this approach is widely used in the previous studies (Bei et al., 2025; Ding et al., 2019; Wu et al., 2018), the quantitative ARIs effects reported here may contain some uncertainty, particularly in regions with strong aerosol-cloud-radiation feedbacks. Nevertheless, the robust regional contrast in precipitation responses that enhancement in the GZB versus suppression in the GZBs is substantially larger than the estimated uncertainty due to nonlinearities, and the qualitative conclusions of this study remain robust. Future work employing incremental aerosol perturbations or partial radiative perturbation techniques could provide a more refined separation of the ARIs effects.*"

9 Comment: The use of a wide range of anthropogenic emission scaling factors (AESF from 1/8 to 8) raises concerns regarding the realism of the experimental design. Such extreme perturbations may not represent realistic atmospheric conditions and could lead to artificial nonlinear responses, including the reported threshold behavior. A justification based on observed aerosol variability is needed.

Response: We have added discussions based on observed aerosol variability in lines 132-144 in the revised manuscript as follow,

"*It is worth noting the use of a wide range of AESFs might not represent realistic emission-control scenarios. In the study, the main purpose of applying a wide range of AESFs is to systematically explore the nonlinear responses of aerosol-cloud-precipitation interactions across aerosol environments ranging from relatively clean to heavily polluted conditions. Wintertime $PM_{2.5}$ concentrations in northern China exhibit substantial variability associated with haze development, boundary-layer evolution, and unfavorable meteorological conditions, often varying by more than one order of magnitude between clean and polluted periods (Li et al., 2021). In the GZB, frequent severe winter haze events have been reported under stagnant meteorological conditions and complex basin topography, with $PM_{2.5}$ concentrations commonly exceeding 200-300 μg m^{-3} during polluted episodes (Bei et al., 2017b). As shown in Figure S1, the average wintertime [$PM_{2.5}$] have decreased from about 160 μg m^{-3} in 2013 to 65 μg m^{-3} in 2026 in response to emission-control measures, highlighting the large variability of aerosol loading in this region. Therefore, the selected AESF range is designed to span the observed variability of aerosol conditions and to identify potential threshold* *and nonlinear behaviors of ARIs and ACIs under different pollution regimes."*

Li, Q., Zhang, H., Cai, X., Song, Y., and Zhu, T.: The impacts of the atmospheric boundary layer on regional haze in North China, npj Clim. Atmos. Sci., 4, 9, https://doi.org/10.1038/s41612-021-00165-y, 2021.

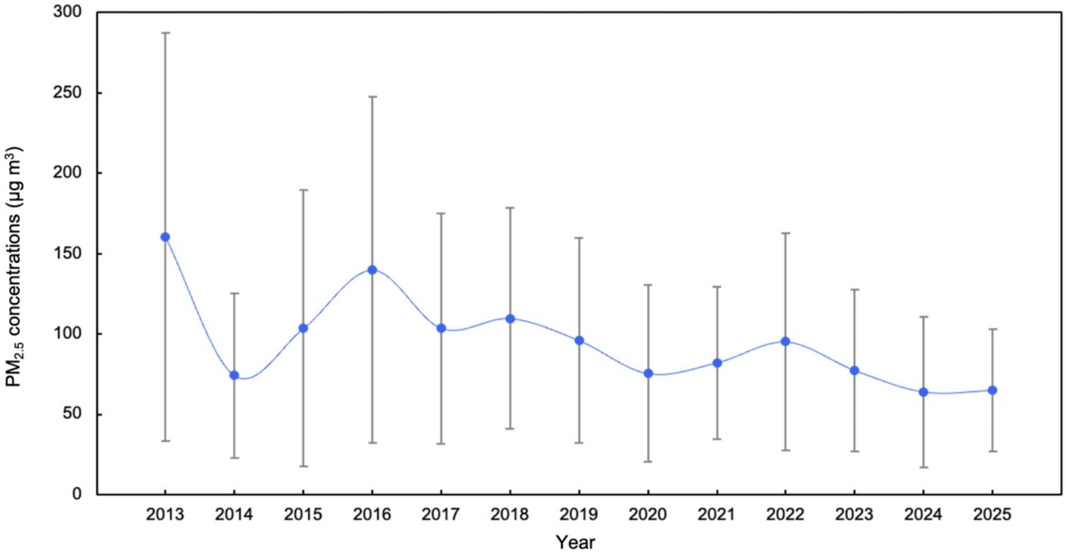

Figure S1: *Interannual variations in observed average [$PM_{2.5}$] over the GZB during the winters (December–January–February) of 2013–2025. The blue circles represent basin-averaged [$PM_{2.5}$], and the error bars indicate the standard deviation among monitoring sites.*